
Chi-Geometry: A Library for Benchmarking Chirality Prediction of GNNs

Rylie Weaver

Computational Sciences and Engineering Division
Oak Ridge National Laboratory
Oak Ridge, TN 37830
weaverre@ornl.gov

Massamiliano Lupo Pasini

Computational Sciences and Engineering Division
Oak Ridge National Laboratory
Oak Ridge, TN 37830
lupopasini@ornl.gov

Abstract

We introduce Chi-Geometry – a library that generates graph data for testing and benchmarking GNNs’ ability to predict chirality. Chi-Geometry generates synthetic graph samples with (i) user-specified geometric and topological traits to isolate certain types of samples and (ii) randomized node positions and species to minimize extraneous correlations. Each generated graph contains exactly one chiral center labeled either R or S, while all other nodes are labeled N/A (non-chiral). The generated samples are then combined into a cohesive dataset that can be used to assess a GNN’s ability to predict chirality as a node classification task. Chi-Geometry allows more interpretable and less confounding benchmarking of GNNs for prediction of chirality in the graph samples which can guide the design of new GNN architectures with improved predictive performance. We illustrate Chi-Geometry’s efficacy by using it to generate synthetic datasets for benchmarking various state-of-the-art (SOTA) GNN architectures. The conclusions of these benchmarking results guided our design of two new GNN architectures. The first GNN architecture established all-to-all connections in the graph to accurately predict chirality across all challenging configurations where previously tested SOTA models failed, but at a computational cost (both for training and inference) that grows quadratically with the number of graph nodes. The second GNN architecture avoids all-to-all connections by introducing a virtual node in the original graph structure of the data, which restores the linear scaling of training and inference computational cost with respect to the number of nodes in the graph, while still ensuring competitive accuracy in detecting chirality with respect to SOTA GNN architectures.

1 Introduction

Materials and molecular structures naturally map onto graphs, where atoms are represented as nodes and interatomic bonds as edges. Because of this natural mapping, graph neural networks (GNNs) reduce the cumbersome and tedious processes of input feature engineering, which is essential for other types of Deep Learning (DL) models, making them the tool of choice for predicting a wide variety of properties at the atomic scale. By predicting scientifically relevant structural and atomic properties, GNNs facilitate research and development in chemistry and materials science. As a result, they

have important downstream applications in healthcare (drug design), technology (battery materials, semiconductors), sustainability (biodegradable materials), infrastructure (composites, alloys), and agriculture (fertilizers, pesticides).

Various material and molecular properties strongly depend on chirality. Three examples with important practical applications are: (i) binding affinity [Morehead and Cheng, 2022, Gaiński et al., 2023], (ii) electronic circular dichroism [Li et al., 2025], and (iii) toxicity [Cremer et al., 2023]. To accurately predict these properties, it is crucial for GNNs to correctly capture the chirality of an atomic structure. High-quality benchmarks are critical to guide the development of new, robust GNN models because they allow the research community to identify shortcomings of existing GNN architectures and propose new GNN architectures to overcome them. However, current datasets for benchmarking chirality prediction have serious limitations. Firstly, there is no straightforward way to isolate data samples with geometric and topological traits that are relevant to a GNN’s predictive ability. Isolating relevant traits, such as the hop distance between the nodes that determine a structure’s chirality, enables targeted testing and thereby more interpretable results for analyses of GNN prediction failures. Secondly, current benchmark datasets contain extraneous correlations that GNNs may inadvertently use when making predictions. This may produce misleading results where a GNN records high performance on the benchmark without learning the function of chirality. Traits that may have extraneous correlations with the benchmarking data are chemical composition, atomic numbers, and interatomic distances/angles.

To address these limitations, we developed Chi-Geometry, a library that generates graphs for testing GNNs’ ability to predict chirality. Chi-Geometry enables targeted testing by generating datasets composed exclusively of samples with user-specified geometric and topological traits, while minimizing extraneous correlations by randomizing node species and positions. To avoid the injection of extraneous correlations in the data, Chi-Geometry generates synthetic graph samples without taking chemical constraints into consideration. As a result, the edges of the generated graph samples do not have chemical meaning and therefore cannot be easily deduced from nodes attributes (e.g., atom types and number of valence electrons for each atom). In contrast, material and molecular graphs typically feature chemically meaningful bonds that are “learnable” from atomic properties. This distinction is crucial for benchmarking GNN architectures that establish all-to-all connections in the graph (e.g., SE(3)-transformer¹ and global E3NN). In fact, when these models are used on chemical data, they can implicitly reconstruct the original connectivity of the graph samples using the chemically meaningful nodal features. However, such retrievability cannot be performed when the graph samples are synthetically generated by Chi-Geometry because the input graph samples do not consider the chemistry. Therefore, GNN architectures that establish all-to-all connections in the graph must explicitly keep track of the original graph topology to succeed in benchmarking tests where data is synthetically generated with the Chi-Geometry library.

We illustrate the effectiveness of Chi-Geometry by benchmarking the ability of several widely used state-of-the-art (SOTA) GNNs to model chirality. In doing so, we find that Chi-Geometry eliminates a previously observed confounding result (Section 4.1) and yields more interpretable results, which facilitates root-cause-analyses of why SOTA GNNs fail to predict chirality (Section 4). Based on the shortcomings identified, we propose two new GNN architectures. Both are equivariant to reflections². The first GNN architecture proposed uses global (all-to-all) connections and engineered edge features that preserve the original graph topology, which attains high accuracy across challenging configurations where previous models failed. Its ability to learn long-range interactions while including global connections is reasonably expected, since global connections artificially convert all long-range interactions into direct, short-range ones. However, its computational cost scales quadratically with the number of nodes, which is undesirable for large graph structures. To mitigate the computational cost while preserving the capability to model long-range interactions, inspired by existing work [Okabe et al., 2024, Sestak et al., 2024, Zhang et al., 2024, Xia et al., 2025], we introduce a second GNN architecture that replaces global connections with the inclusion of a virtual node in the original graph, which is then connected to all the other nodes to accelerate exchange of information across the graph topology. While incorporating a virtual node partially sacrifices accuracy

¹Since there is a mathematical equivalence between the self-attention mechanism in Transformers and all-to-all message passing in GNNs [El et al., 2025], Transformers fall within our broader investigation of GNN architectures.

²Although invariance is formally a special case of equivariance (see Appendix C), we use “equivariant” to concisely refer to models that are equivariant but not invariant.

compared to the globally connected model, it maintains linear computational scaling. Notably, it is the only GNN we test that is able to detect long-range chirality with better-than-random accuracy while scaling linearly. To the best of our knowledge, this is the first study where the technique of virtual graph nodes is used for chirality predictions. Our numerical results suggest a path towards developing accurate and computationally efficient GNN models that capture global chirality, which presents an intriguing direction for future research. The identification of such a class of GNN models with judicious balance between training cost and accuracy is relevant for real-world computational chemistry applications.

The remainder of the paper is organized as follows. In Section 2, we provide background on chirality and chirality prediction with GNNs. In Section 3, we explain the configurational options that dictate dataset generation in Chi-Geometry. In Section 4, we benchmark various SOTA GNN architectures, taking advantage of Chi-Geometry’s targeted testing and improved interpretability to pinpoint each architecture’s shortcomings. Using these insights, we then develop two new GNN architectures. The first architecture predicts chirality with high accuracy across all challenging configurations where the other SOTA models failed, but scales quadratically with the number of nodes, while the second architecture strikes a balance between computational efficiency and accuracy and provides a promising direction for future research. Lastly, in Section 5, we provide concluding remarks.

2 Background

2.1 Chirality

An object O is chiral if there exists no combination of rotations and translations that maps O onto its mirror image O' . As a result, there is a 1-to-1 correspondence between chirality and reflection-orientation. Mathematically, this is expressed as:

$$\forall \text{ transformations } \mathbb{T} \in \text{SE}(3), \mathbb{T}(O) \neq O'$$

In chemical contexts, the Cahn-Ingold Prelog (CIP) priority rules are a common procedure for identifying chiral centers and determining their chirality tags [Favre and Powell, 2013]. To illustrate, the process goes as follows:

1. Identify Chiral Centers: An atom (node) with four unique neighbors is considered a potential chiral center (labeled ‘c’ in Figure 1). Otherwise, the atom is labeled N/A.
2. Assign Priorities: Rank the four neighbors from highest to lowest by atomic number. If two or more neighbors share the same atomic number, continue by recursively comparing node attributes, edge attributes, etc, until all neighbors are unequivocally differentiated (stop and label the node N/A if the neighbors cannot be differentiated).
3. Orient the Atomic Structure: Position the atomic structure so that the neighbor with the lowest priority points away from the viewer, behind the chiral center.
4. Determine Chirality: Trace the path along the 1st, 2nd, and 3rd highest-priority neighbors. If the path from $1 \rightarrow 2 \rightarrow 3$ is clockwise, label the center as R; if it is counterclockwise, label it as S (label N/A if there is no clockwise or counterclockwise orientation) (see Figure 1 for examples)

2.2 GNNs for Chirality Prediction

Convolutional GNNs [Kipf and Welling, 2017] (a.k.a. message-passing GNNs), in particular, have been shown to effectively model the complex relational structures of graphs via message-passing layers [Duvenaud et al., 2015, Gilmer et al., 2017, Schütt et al., 2017, Hamilton et al., 2018, Veličković et al., 2018, Gasteiger et al., 2024, Chen et al., 2019, Lupo Pasini et al., 2022, Batzner et al., 2022, Batatia et al., 2022, Chen and Ong, 2022, Liao and Smidt, 2022, Liao et al., 2024]. Most GNN architectures cannot to predict chirality on graphs, because their representation of different chiral forms is identical. However, some architectures have been developed to include chirality prediction as a capability [Morehead and Cheng, 2022, Gaiński et al., 2023, Adams et al., 2021, Liu et al., 2022]. Specifically, GNNs have been applied to predict properties that depend critically on molecular chirality. An example is the binding affinity [Morehead and Cheng, 2022, Gaiński et al., 2023], which

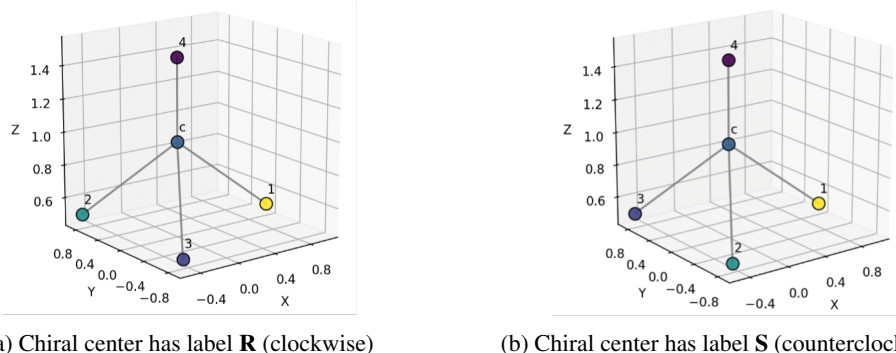


Figure 1: Example of mirrored chiral structures. The chiral center is labeled ‘c’, and its neighbors are labeled numerically according to their priority.

measures the strength of a molecule’s bond to a biological target (e.g., small organic molecule binding to a large protein structure). Another example is toxicity [Cremer et al., 2023], where the chiral form a molecule takes may drastically change both its intended and/or side effects when used as a drug. A final example is electronic circular dichroism (ECD) [Li et al., 2025], which refers to the differential absorption of left and right polarized light. ECD is highly relevant to the discovery and development of new optical materials. However, many stereochemical assignments rely on long-range structural relationships that GNNs struggle to accurately capture [Bengio et al., 1994, Pascanu et al., 2013, Alon and Yahav, 2021, Rusch et al., 2023]. For example, the CIP procedure for labeling a stereocenter (Section 2.1) may depend on nodes that are multiple connection hops away from the chiral center if the immediate neighbors of a chiral center have equivalent traits (e.g. atomic number). Another example arises in axially chiral systems, such as allenes and cumulenes, where chirality is determined by the relative angular orientation of substituents separated by multiple double bonds (for example, 1,3-diphenylallene). Batatia et al. [2024] specifically employed cumulenes to show that accurately predicting force-field energies requires GNNs capable of modeling these long-range interactions. But, message-passing GNN architectures with K message-passing layers cannot propagate information beyond K hops [Li et al., 2018]. Moreover, although arbitrarily deep networks can theoretically propagate information from arbitrarily many hops away, they encounter several computational challenges. First, over-smoothing causes node embeddings to converge toward indistinguishable vectors, degrading their utility for downstream tasks [Rusch et al., 2023]. Second, deep GNNs are prone to vanishing or exploding gradients, which hinder effective training [Bengio et al., 1994, Pascanu et al., 2013]. Finally, over-squashing arises when exponentially larger neighborhoods are compressed into fixed-size representations, attenuating the very long-range signals that deeper layers aim to capture [Alon and Yahav, 2021].

Since long-range dependencies influence chirality assignments and are poorly captured by standard GNNs, it is important to construct test sets that emphasize these interactions when evaluating model robustness. However, existing benchmarks neither permit the selective sampling of molecules according to specific geometric or topological criteria nor avoid spurious correlations that can obscure a model’s true capabilities. For example, Morehead and Cheng [2022] found that the DimeNet++ architecture was able to classify a chiral molecule’s chirality as R or S with 65.7% accuracy. This result is surprising because the architecture in question uses exclusively the atomic number, pairwise distances, and triplet angles as inputs, all of which do not change under reflection. Consequently, the representations are identical for two mirror-image atomic structures, which should imply near-random (i.e., 50%) accuracy for R/S chirality classification. Yet, its accuracy significantly exceeded random chance, which suggests that the model used extraneous correlations to predict chirality. The lack of targeted datasets that minimize extraneous correlations, which lead to confounding results like the one mentioned above, is the motivation behind developing Chi-Geometry, a library for generating randomized chiral graphs with explicit control over relevant geometric/topological features.

3 Chi-Geometry

The dataset generation of Chi-Geometry is parametrized by the following arguments: **Chirality Distance**, **Chirality Type**, **Species Range**, and **Noise**. The Chirality Distance and Chirality Type parameters control the topological/geometric features of the generated dataset, as illustrated by Figure 2 and explained in Appendix B. Additionally, Chi-Geometry reduces the effect of potential extraneous correlations by randomly assigning the node species (always) and positions (when Noise = True). Lastly, the species range varies the degree of difficulty of the preliminary sorting task that is required to predict chirality, which is useful for faster testing and development. In each structure, there is exactly one node that is a chiral center with label R or S (see details in Appendix B). Below, we briefly elaborate on how the configurational parameters dictate sample generation.

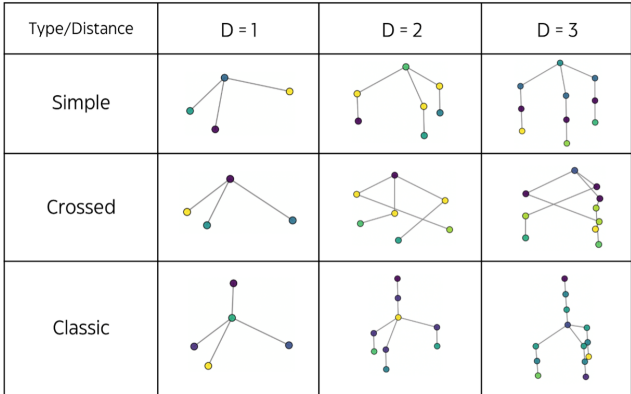


Figure 2: Examples of the Simple, Crossed, and Classic configuration types in Chi-Geometry at distances 1, 2, and 3 with species range 15 and noise = False.

Chirality Distance: Specifies how many connection ‘hops’ the chiral relationship spans by adding (d-1) intermediate ‘layers’³ in between the chiral center and the nodes that determine its chirality, which is crucial for testing the robustness of the GNN’s ability to learn long-range interactions that determine the chirality.

Chirality Type: Provides three choices for structural arrangements of chiral configurations: Simple, Crossed, and Classic, each testing different aspects of the GNN’s ability to learn chirality. The classic and simple types test the GNN’s ability to learn from variable-range node attributes and local geometry. On the other hand, the crossed type tests the GNN’s ability to learn from variable-range node attributes and geometry (Appendix B.3). Since chirality is determined by both node attributes and geometry, we constructed the sample types to span a comprehensive set of attribute-geometry combinations. As a result, the available sample types capture nearly all structural configurations of interest for testing chirality prediction. Additionally, the classic type more closely represents the types of chiral centers found in chemistry (four neighbors), while the simple type is the minimal configuration needed to fit the formal definition of chirality (three neighbors). To provide a more complete set of options to users with different needs and preferences, we included both.

Species Range: For each generated chiral structure, the integer node species are selected randomly and uniformly from the set $\{1, 2, \dots, \text{species range}\}$. Some nodes may be constrained to share the same node species, but all the selected node species are chosen at random. So, the species range parameter sets the upper bound for the integer selection. As explained in (Section 2.1) and Appendix B, labeling a chiral center requires ranking nodes based on their attributes. By varying the species range parameter, users can adjust the complexity of this ranking task that the GNN must learn. By setting a reasonably small species range, users can test chirality prediction for GNNs without requiring a large dataset for the GNN to learn large-scale sorting. This is useful for running quicker tests during development.

³The ‘layers’ of samples are unrelated to the convolutional layers of graph neural networks. Refer to Figure 2 for an illustration of increasing layers as the chirality distance increases, or Appendix B for an explanation of layer generation.

Noise: If noise = True, the positions of the nodes will be randomly assigned. This randomization is useful to reduce the effect of extraneous correlations, while noise = False is clearer for visualization.

4 Benchmarking Results

By specifying Chi-Geometry’s chirality distance parameter, we systematically tested several widely used GNN architectures on their ability to identify chirality at specified hop distances (see Appendix A for more details on the dataset, model, and training parameters). For each GNN architecture, we evaluated performance on homogeneous datasets where chirality is consistently determined by nodes that are all at hop distance D from the chiral center. First, we train and evaluate an architecture on a dataset with $D = 1$. If a model does not achieve high accuracy, we repeat the experiment nine more times (10 runs total) to verify the result and produce error bars. If a model succeeds at $D = 1$, we extend evaluation to datasets with hop distances $D = 2 - 9$ and do not repeat the runs because of the computational cost. All models used the same datasets for each respective D value. The homogeneity of the datasets in our tests yields more interpretable results, which we used to develop two new architectures that perform better across the challenging configurations where the other models failed. Specifically, we tested five existing architectures—DimeNet++ [Gasteiger et al., 2022], Vanilla MPNN, SE(3)-Transformer [Wang, 2024], E3NN⁴ with global connections [Geiger et al., 2022], and E3NN with local connections [Geiger et al., 2022]—as well two developed architectures—E3NN with global connections and feature engineering [Geiger et al., 2022] and E3NN with virtual node [Geiger et al., 2022].

The tested models include those that are equivariant to reflections (all E3NN models), those that are invariant to reflections (DimeNet++, SE(3)-Transformer) (Appendix C), and those that are neither invariant nor equivariant (Vanilla MPNN). Additionally, the tested models include various connectivity types (global, original, virtual node). Thus, our selection of tested models collectively spans a broad spectrum of architectural designs relevant to chirality prediction.

The number of message-passing layers was chosen to ensure sufficient receptive field given each model’s connectivity and the value of D . For models using the original adjacency (DimeNet++, Vanilla MPNN, Local E3NN), we set layers = $D + 3$ because preliminary experiments showed four layers sufficed to predict chirality at $D = 1$ with the Local E3NN architecture, and we infer that the number of required layers will increase correspondingly with D . For architectures that use all-to-all connections (Global E3NN, E3NN with Virtual Node, SE(3)-Transformer) and thereby reduce the hop distance between nodes in the graph, we use four layers.

4.1 Existing Architectures

We examine five existing architectures on their ability to classify chirality, which are listed below:

As shown in Table 2, the DimeNet++, Vanilla MPNN, SE(3)-Transformer, and Global E3NN architectures failed to predict chirality with high accuracy at $D = 1$. Both the DimeNet++ and SE(3)-Transformer models distinguished R or S chiral centers at no better than random, as expected given their reflection invariance (Appendix C), which precludes any representation of chirality.

While the Vanilla MPNN is not reflection-invariant and therefore, in principle, should be capable of predicting chirality, it performed no better than random when classifying chiral centers as R or S. This highlights practical limitations of GNN architectures in modeling chirality, despite their theoretical capability to do so. Both the SE(3)-Transformer and Global E3NN models struggled to classify non-chiral centers as N/A, which we attribute to losing clear topological indicators for which node is a chiral center when rewiring the graph with global connections. Again, we emphasize that in real-world molecular and materials datasets typically have chemically meaningful bonds that the GNN may be able to learn. However, this is not true for graphs generated by Chi-Geometry because they are randomized to reduce extraneous correlations. In predictive tasks where the edges

⁴The e3nn library (MIT license) [Geiger et al., 2022] is an open-source software for building equivariant neural networks. For our analysis, we use the January 2021 release of its example model.

⁵The open-source PyTorch Implementation of the SE(3)-Transformer (a.k.a. Equiformer or Equivariant Transformer) [Wang, 2024] draws on previous publications from Lee et al. [2022], Shazeer [2019], Ding et al. [2021], Kim et al. [2020], Zitnick et al. [2022], Passaro and Zitnick [2023], Gomez et al. [2017], Bondarenko et al. [2023], Arora et al. [2023].

Model	Architectural Details
DimeNet++ [Gasteiger et al., 2022]	Includes pairwise distances and triplet angles in message-passing.
Vanilla MPNN	Relies on a pairwise message-passing layer without equivariance to reflections, which is shared across many models (e.g., GCNN [Gilmer et al., 2017], SAGE [Hamilton et al., 2018], MFC [Duvenaud et al., 2015], GATv2 [Brody et al., 2022]). Node positions are appended directly to the node features to ensure that the model is theoretically capable of modeling chirality.
SE(3)-Transformer [Wang, 2024] ⁵	Equivariant to rotations and translations and has shown strong performance on structural and atomic prediction tasks [Liao and Smidt, 2022, Fuchs et al., 2020, Barroso-Luque et al., 2024].
E3NN (two variants: Local, Global) [Geiger et al., 2022]	The e3nn library has been used to develop several notable GNNs [Batzner et al., 2022, Batatia et al., 2022]. We use the e3nn library to construct GNN architectures that are equivariant to reflections, and thereby are able to detect chirality (Appendix C). We evaluate two variants: the local model which uses the original graph adjacency, and the global model which rewires the graph for all-to-all connections.

Table 1: The existing architectures which are tested with Chi-Geometry and their details.

Class	DimeNet++ (D=1)	Vanilla MPNN (D=1)	SE(3)-Transformer (D=1)	Global E3NN (D=1)
N/A	100% \pm 0%	100% \pm 0%	79% \pm 1%	76% \pm 2%
R	51% \pm 18%	58% \pm 9%	38% \pm 19%	65% \pm 2%
S	49% \pm 18%	42% \pm 9%	41% \pm 19%	66% \pm 2%

Table 2: Classification accuracy of the DimeNet++, Vanilla MPNN, SE(3)-Transformer, and Global E3NN architectures at hop distance $D = 1$ over 10 repetitions with standard deviation error bars.

are learnable by the GNN, the SE(3)-Transformer and E3NN model with global connections may perform better, although we expect the SE(3)-Transformer to always predict chiral centers as R or S no better than random because of its reflection invariance (Appendix C).

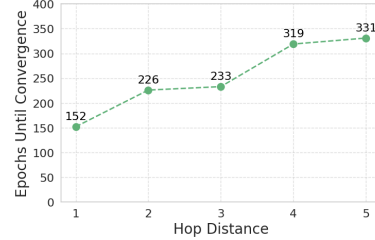
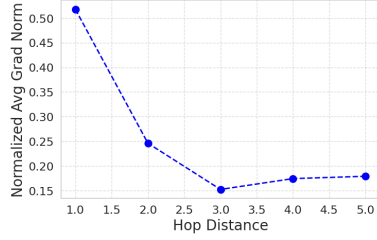
These results highlight two key contributions from Chi-Geometry. First, it eliminates the confounding result reported by [Morehead and Cheng, 2022], where DimeNet++ classified chirality at above random accuracy despite being reflection-invariant (Section 2.2). Second, it shows that the Vanilla MPNN fails to learn chirality even in the simplest setting ($D = 1$) despite architecture’s theoretical capacity to model chirality, which was not obvious a-priori.

Class	D=1	D=2	D=3	D=4	D=5	D=6	D=7	D=8	D=9
N/A	100%	94%	97%	92%	92%	56%	26%	44%	39%
R	95%	65%	77%	68%	69%	16%	64%	33%	38%
S	99%	33%	21%	31%	29%	20%	15%	20%	29%

Table 3: Classification accuracy of the Local E3NN architecture at hop distances $D = 1$ -9.

The Local E3NN model achieved high prediction accuracy for $D = 1$ but degrades rapidly for higher distances Table 3. This is in line with well-established limitations of deep GNNs, namely their difficulty in capturing long-range dependencies [Rusch et al., 2023, Li et al., 2018, Topping et al., 2022, Alon and Yahav, 2021] and vanishing and/or exploding gradients [Bengio et al., 1994, Pascanu et al., 2013]. At $D \geq 6$, the model encounters training instabilities including returning losses of inf and gradients of NaN, despite gradient clipping in the training stage. We also found strong indications of over-squashing [Topping et al., 2022, Alon and Yahav, 2021] via the normalized average gradient of node features with respect to the chiral center’s classification loss (Appendix D). As seen in Figure 3a, the gradients of the node features which determine a chiral center’s tag diminished as their hop distance from the chiral center increased, despite the importance of these features for the classification. Additionally, the training took more epochs to converge as D increased (Figure 3b), suggesting that there are more instabilities and/or weaker signals that delay convergence for larger hop distances.

Overall, we see indications that the Local E3NN model architecture struggles to learn chirality at hop distances greater than 1 due to over-squashing, weak training signals, and instability.



(a) Normalized average gradient of node features that determine the chiral center’s tag, as a function of hop distance. (b) Epochs required for convergence by hop distance.

Figure 3: Indicators of over-squashing and extended training times as hop distance increases.

4.2 Developed Architectures

Based on these results, we developed two new architectures designed to address all the limitations discussed in Section 4.1. Namely, the shortcomings are that: (1) DimeNet++, the General MPNN, and the SE(3)-Transformer do not detect reflections, (2) the E3NN model with local connections exhibited over-squashing and training instabilities, and (3) the E3NN model with global connections and the SE(3)-Transformer lose topological information during graph rewiring.

The first model we developed is an E3NN model with global connections and judiciously engineered edge features that preserve the original graph topology. The second model is an E3NN model with a virtual node. Both models are equivariant to reflections (and therefore chirality) by construction (Appendix C). The global connections mitigate over-squashing [Alon and Yahav, 2021, Topping et al., 2022] by providing direct, all-to-all connections that avoid long-range bottlenecks. Although all long-range information still must pass through a single virtual node (creating a bottleneck), using a virtual node reduces the number of edges that information must propagate through to reach distant nodes, thereby mitigating over-squashing. Also, both models use only four message-passing layers, thereby minimizing vanishing and/or exploding gradients which often arise in deep networks [Álvaro Arroyo et al., 2025, Pascanu et al., 2013].

4.2.1 E3NN with Global Connections and Feature Engineering

Firstly, we developed an E3NN model with global connections that was adjusted to include judiciously engineered edge features which preserve the original graph topology. Specifically, we use (1) the shortest-path hop distance under the original adjacency, and (2) a one-hot encoding denoting whether that edge existed in the original graph. By preserving the original graph topology via the edge features, the network learns to disambiguate the chiral center even after rewiring with global connections.

Class	D=1	D=2	D=3	D=4	D=5	D=6	D=7	D=8	D=9
N/A	100%	100%	100%	100%	100%	100%	99%	100%	100%
R	100%	98%	100%	98%	100%	99%	98%	100%	100%
S	100%	98%	100%	97%	100%	100%	98%	99%	99%

Table 4: Classification accuracy of an E3NN model with global connections and feature engineering.

As shown in Table 4, the E3NN model with this combination of global connections and judiciously designed edge features predicts chirality with high accuracy on all configuration types that we previously used to test the other models. However, it is important to highlight that the model’s successful capture of long-range interactions is not particularly surprising given its global (all-to-all) connectivity, which scales quadratically with the number of nodes and naturally facilitates information flow across any hop distance. Additionally, the engineered features preserving the original graph topology were necessary specifically because Chi-Geometry generates synthetic graphs where edges cannot be inferred from node attributes alone. Nevertheless, this model’s performance confirms Chi-Geometry’s capability as a practical benchmark: it identifies whether models can effectively learn to predict chirality on graph-structured data, especially in difficult samples with long-range interactions, thereby guiding future model improvements.

4.2.2 E3NN with Virtual Node

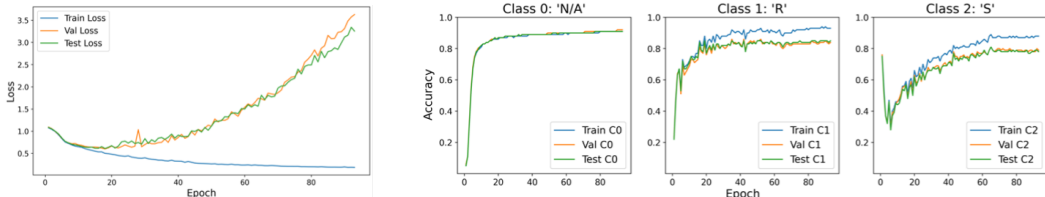
Second, we developed an E3NN model with a virtual node to attempt to capture long-range interactions that determine the chirality while scaling linearly with the number of nodes. A virtual node is an

additional node, not part of the original graph, that receives messages from all other nodes (all-to-one) and sends messages back to them (one-to-all). Message-passing with a virtual node scales linearly with the number of nodes in a graph. Additionally, previous studies have shown that, in principle, message passing neural networks (MPNNs) with virtual node can, arbitrarily approximate the self-attention layer of an all-to-all message passing model (Graph Transformer). Given (i) the success of the all-to-all message-passing model in Section 4.2.1, (ii) the previous work establishing the ability for virtual nodes to approximate all-to-all message passing, and (iii) the favorable computational scaling of a virtual node as opposed to all-to-all message-passing, we view it as a natural next step to study the chirality prediction capability of an E3NN model with a virtual node. Prior work has used virtual nodes in other settings than chirality prediction [Okabe et al., 2024, Sestak et al., 2024, Zhang et al., 2024, Xia et al., 2025]. However, to our knowledge, this is the first study that (i) uses a virtual node which is equivariant to reflections and (ii) applies a virtual node architecture to chirality prediction.

Class	D=1	D=2	D=3	D=4	D=5	D=6	D=7	D=8	D=9
N/A	84%	87%	77%	75%	63%	68%	56%	85%	66%
R	99%	78%	61%	55%	55%	42%	57%	45%	62%
S	92%	57%	40%	42%	43%	54%	41%	45%	39%

Table 5: Classification accuracy of an E3NN model with a virtual node.

The E3NN model with a virtual node yields promising results, achieving better-than-random classification of R/S chiral centers at $D = 2$ Table 5. Notably, no other model that we tested achieves better than random R/S accuracy at $D = 2$ while computationally scaling linearly with the number of nodes. These results suggest that the virtual node architecture offers a promising trade-off: while not as accurate as the global model, it provides improved performance over other linearly-scaling models at intermediate distances with significantly reduced computational cost.



(a) Train/val/test loss over epochs for $D = 2$.

(b) Classification accuracy by class for train/val/test over epochs at $D = 2$.

The training dynamics for $D = 2$ shown in Figures 4a and 4b help explain these failures and offer avenues for future study. The model reaches its minimum validation loss at epoch 18, but both validation and test accuracies continue rising beyond that epoch. We ascribe this counterintuitive behavior to the model confidently misclassifying a minority of the samples, despite improving on most. At the last epoch, the model’s train/test accuracies are [0.91,0.93,0.88] and [0.91,0.85,0.78], respectively, which is not captured in Table 5 because of early-stopping. We observed similar behavior for all $D = 1-9$. Overall, these results suggest that although the current virtual-node E3NN does not beat random guessing on R/S classification for $D > 2$, systematic architectural and algorithmic refinements (e.g. entropy regularization) could yield a variant that retains linear scaling with accuracy competitive to the more expensive global models.

5 Conclusions

We have presented Chi-Geometry, a library that generates datasets for testing and benchmarking chirality prediction of GNNs. Chi-Geometry allows users to select structurally relevant geometric and topological traits and reduces the effect of extraneous correlations in its dataset generation. By allowing users to select structural features of interest for targeted testing, Chi-Geometry gives more interpretable results for a root-cause analysis of prediction failures. Additionally, by reducing the effect of extraneous correlations, Chi-Geometry minimizes confounding results whereby a model seems to perform well despite not actually learning the function of chirality. Using Chi-Geometry datasets, we illustrated the limitations of several widely used SOTA GNN models to classify chirality on graphs. Specifically, we identified over-squashing/training instability, lack of chirality representation, and information loss in graph rewiring as root causes of prediction failures. In addition, we used the insights drawn from our targeted tests to develop two new architectures –

an E3NN model with global connections and engineered edge features and an E3NN model with a virtual node – which show improved performance on the challenging configurations where other models failed to predict chirality. Overall, Chi-Geometry generates targeted datasets for testing and benchmarking, producing more interpretable and less confounding results, thereby facilitating the development of improved GNN architectures for chirality prediction.

References

- Keir Adams, Lagnajit Pattanaik, and Connor W. Coley. Learning 3d representations of molecular chirality with invariance to bond rotations, 2021. URL <https://arxiv.org/abs/2110.04383>.
- Uri Alon and Eran Yahav. On the bottleneck of graph neural networks and its practical implications. *arXiv preprint arXiv:2006.05205*, 2021. URL <https://doi.org/10.48550/arXiv.2006.05205>.
- Simran Arora, Sabri Eyuboglu, Aman Timalsina, Isys Johnson, Michael Poli, James Zou, Atri Rudra, and Christopher R’e. Zoology: Measuring and improving recall in efficient language models. 2023. URL <https://api.semanticscholar.org/CorpusID:266149332>.
- Luis Barroso-Luque, Muhammed Shuaibi, Xiang Fu, Brandon M. Wood, Misko Dzamba, Meng Gao, Ammar Rizvi, C. Lawrence Zitnick, and Zachary W. Ulissi. Open materials 2024 (omat24) inorganic materials dataset and models. *arXiv preprint arXiv:2410.12771*, 2024. URL <https://doi.org/10.48550/arXiv.2410.12771>.
- Ilyes Batatia, Dávid P. Kovács, Gregor N. C. Simm, Christoph Ortner, and Gábor Csányi. Mace: Higher order equivariant message passing neural networks for fast and accurate force fields. *arXiv preprint*, 2022. URL <https://doi.org/10.48550/arXiv.2206.07697>.
- Ilyes Batatia, Lars L. Schaaf, Huajie Chen, Gábor Csányi, Christoph Ortner, and Felix A. Faber. Equivariant matrix function neural networks. In *International Conference on Learning Representations (ICLR)*, 2024. URL <https://doi.org/10.48550/arXiv.2310.10434>.
- Simon Batzner, Albert Musaelian, Lixin Sun, and et al. E(3)-equivariant graph neural networks for data-efficient and accurate interatomic potentials. *Nature Communications*, 13:2453, 2022. doi: 10.1038/s41467-022-29939-5.
- Yoshua Bengio, Patrice Simard, and Paolo Frasconi. Learning long-term dependencies with gradient descent is difficult. *IEEE transactions on neural networks*, 5(2):157–166, 1994.
- Yelysei Bondarenko, Markus Nagel, and Tijmen Blankevoort. Quantizable transformers: Removing outliers by helping attention heads do nothing. *ArXiv*, abs/2306.12929, 2023. URL <https://api.semanticscholar.org/CorpusID:259224568>.
- Shaked Brody, Uri Alon, and Eran Yahav. How attentive are graph attention networks?, 2022. URL <https://arxiv.org/abs/2105.14491>.
- Chi Chen and Shyue Ping Ong. A universal graph deep learning interatomic potential for the periodic table. *Nature Computational Science*, 2(11):718–728, November 2022.
- Chi Chen, Weike Ye, Yunxing Zuo, Chen Zheng, and Shyue Ping Ong. Graph networks as a universal machine learning framework for molecules and crystals. *Chemistry of Materials*, 31(9):3564–3572, April 2019. ISSN 1520-5002. doi: 10.1021/acs.chemmater.9b01294. URL <http://dx.doi.org/10.1021/acs.chemmater.9b01294>.
- Julian Cremer, Leonardo Medrano Sandomas, Alexandre Tkatchenko, Djork-Arné Clevert, and Gianni De Fabritiis. Equivariant graph neural networks for toxicity prediction. *Chemical Research in Toxicology*, 36(10):1561–1573, 2023. doi: 10.1021/acs.chemrestox.3c00032. URL <https://doi.org/10.1021/acs.chemrestox.3c00032>. PMID: 37690056.
- Ming Ding, Zhuoyi Yang, Wenyi Hong, Wendi Zheng, Chang Zhou, Da Yin, Junyang Lin, Xu Zou, Zhou Shao, Hongxia Yang, and Jie Tang. Cogview: Mastering text-to-image generation via transformers, 2021.

- David Duvenaud, Dougal Maclaurin, Jorge Aguilera-Iparraguirre, Rafael Gómez-Bombarelli, Timothy Hirzel, Alán Aspuru-Guzik, and Ryan P. Adams. Convolutional networks on graphs for learning molecular fingerprints, 2015. URL <https://arxiv.org/abs/1509.09292>.
- Batu El, Deepto Choudhury, Pietro Liò, and Chaitanya K. Joshi. Towards mechanistic interpretability of graph transformers via attention graphs, 2025. URL <https://arxiv.org/abs/2502.12352>.
- Henri A Favre and Warren H Powell. *Nomenclature of Organic Chemistry*. The Royal Society of Chemistry, 12 2013. ISBN 978-0-85404-182-4. doi: 10.1039/9781849733069. URL <https://doi.org/10.1039/9781849733069>.
- Fabian B. Fuchs, Daniel E. Worrall, Volker Fischer, and Max Welling. Se(3)-transformers: 3d roto-translation equivariant attention networks. *arXiv preprint arXiv:2006.10503*, 2020. URL <https://doi.org/10.48550/arXiv.2006.10503>.
- Piotr Gaiński, Michał Koziarski, Jacek Tabor, and Marek Śmieja. Chienn: Embracing molecular chirality with graph neural networks. *arXiv preprint arXiv:2307.02198*, 2023. URL <https://doi.org/10.48550/arXiv.2307.02198>.
- Johannes Gasteiger, Janek Groß, and Stephan Günnemann. Directional message passing for molecular graphs, 2022. URL <https://arxiv.org/abs/2003.03123>.
- Johannes Gasteiger, Florian Becker, and Stephan Günnemann. Gemnet: Universal directional graph neural networks for molecules, 2024. URL <https://arxiv.org/abs/2106.08903>.
- Mario Geiger, Tess Smidt, Alby M., Benjamin Kurt Miller, Wouter Boomsma, Bradley Dice, Kostiantyn Lapchevskyi, Maurice Weiler, Michał Tyszkiewicz, Simon Batzner, Dylan Madisetti, Martin Uhrin, Jes Frellsen, Nuri Jung, Sophia Sanborn, Mingjian Wen, Josh Rackers, Marcel Rødd, and Michael Bailey. Euclidean neural networks: e3nn, April 2022. URL <https://doi.org/10.5281/zenodo.6459381>.
- Justin Gilmer, Samuel S. Schoenholz, Patrick F. Riley, Oriol Vinyals, and George E. Dahl. Neural message passing for quantum chemistry. In Doina Precup and Yee Whye Teh, editors, *Proceedings of the 34th International Conference on Machine Learning*, volume 70 of *Proceedings of Machine Learning Research*, pages 1263–1272. PMLR, 06–11 Aug 2017. URL <https://proceedings.mlr.press/v70/gilmer17a.html>.
- Aidan N. Gomez, Mengye Ren, Raquel Urtasun, and Roger Baker Grosse. The reversible residual network: Backpropagation without storing activations. In *NIPS*, 2017.
- William L. Hamilton, Rex Ying, and Jure Leskovec. Inductive representation learning on large graphs, 2018. URL <https://arxiv.org/abs/1706.02216>.
- John Jumper, Richard Evans, Alexander Pritzel, and et al. Highly accurate protein structure prediction with alphafold. *Nature*, 596(7873):583–589, 2021. doi: 10.1038/s41586-021-03819-2. Published online 15 July 2021.
- Hyunjik Kim, George Papamakarios, and Andriy Mnih. The lipschitz constant of self-attention. In *International Conference on Machine Learning*, 2020.
- Thomas N. Kipf and Max Welling. Semi-supervised classification with graph convolutional networks. *arXiv preprint arXiv:1609.02907*, 2017. doi: 10.48550/arXiv.1609.02907.
- Risi Kondor and Shubhendu Trivedi. On the generalization of equivariance and convolution in neural networks to the action of compact groups. In *Proceedings of the 35th International Conference on Machine Learning (ICML)*, 2018. URL <https://doi.org/10.48550/arXiv.1802.03690>. Stockholm, Sweden. *arXiv preprint: 1802.03690v3*.
- Jae Hyeon Lee, Payman Yadollahpour, Andrew Watkins, Nathan C. Frey, Andrew Leaver-Fay, Stephen Ra, Kyunghyun Cho, Vladimir Gligorijevic, Aviv Regev, and Richard Bonneau. Equifold: Protein structure prediction with a novel coarse-grained structure representation. *bioRxiv*, 2022. doi: 10.1101/2022.10.07.511322. URL <https://www.biorxiv.org/content/early/2022/10/08/2022.10.07.511322>.

- H. Li, D. Long, L. Yuan, and et al. Decoupled peak property learning for efficient and interpretable electronic circular dichroism spectrum prediction. *Nature Computational Science*, 2025. doi: 10.1038/s43588-024-00757-7. URL <https://doi.org/10.1038/s43588-024-00757-7>. Check for updates via CrossMark.
- Qimai Li, Zhichao Han, and Xiao-Ming Wu. Deeper insights into graph convolutional networks for semi-supervised learning, 2018. URL <https://arxiv.org/abs/1801.07606>.
- Yi Liao and Tess E. Smidt. Equiformer: Equivariant graph attention transformer for 3d atomistic graphs. *ArXiv*, abs/2206.11990, 2022.
- Yi-Lun Liao, Brandon Wood, Abhishek Das, and Tess Smidt. Equiformerv2: Improved equivariant transformer for scaling to higher-degree representations, 2024. URL <https://arxiv.org/abs/2306.12059>.
- Yi Liu, Limei Wang, Meng Liu, Xuan Zhang, Bora Oztekin, and Shuiwang Ji. Spherical message passing for 3d graph networks, 2022. URL <https://arxiv.org/abs/2102.05013>.
- Massimiliano Lupo Pasini, Pei Zhang, Samuel Temple Reeve, and Jong Youl Choi. Multi-task graph neural networks for simultaneous prediction of global and atomic properties in ferromagnetic systems. *Machine Learning: Science and Technology*, 3(2):025007, May 2022. ISSN 2632-2153. doi: 10.1088/2632-2153/ac6a51. URL <http://dx.doi.org/10.1088/2632-2153/ac6a51>.
- A. Merchant, S. Batzner, S. S. Schoenholz, and et al. Scaling deep learning for materials discovery. *Nature*, 624:80–85, 2023. doi: 10.1038/s41586-023-06735-9. Published online 29 November 2023, issue date 07 December 2023.
- Alex Morehead and Jianlin Cheng. Geometry-complete perceptron networks for 3d molecular graphs. *arXiv preprint arXiv:2211.02504*, 2022. URL <https://doi.org/10.48550/arXiv.2211.02504>.
- Ryotaro Okabe, Abhijatmedhi Chotrattanapituk, Artittaya Boonkird, Nina Andrejevic, Xiang Fu, Tommi S Jaakkola, Qichen Song, Thanh Nguyen, Nathan Drucker, Sai Mu, Yao Wang, Bolin Liao, Yongqiang Cheng, and Mingda Li. Virtual node graph neural network for full phonon prediction. *Nature Computational Science*, 4(7):522–531, July 2024.
- Razvan Pascanu, Tomas Mikolov, and Yoshua Bengio. On the difficulty of training recurrent neural networks. In *International Conference on Machine Learning (ICML)*, pages 1310–1318. PMLR, 2013.
- Saro Passaro and C. Lawrence Zitnick. Reducing so(3) convolutions to so(2) for efficient equivariant gnns. *ArXiv*, abs/2302.03655, 2023.
- T. Konstantin Rusch, Michael M. Bronstein, and Siddhartha Mishra. A survey on oversmoothing in graph neural networks. *arXiv preprint arXiv:2303.10993*, 2023. doi: 10.48550/arXiv.2303.10993.
- Kristof Schütt, Pieter-Jan Kindermans, Huziel Enoc Saucedo Felix, Stefan Chmiela, Alexandre Tkatchenko, and Klaus-Robert Müller. Schnet: A continuous-filter convolutional neural network for modeling quantum interactions. In I. Guyon, U. Von Luxburg, S. Bengio, H. Wallach, R. Fergus, S. Vishwanathan, and R. Garnett, editors, *Advances in Neural Information Processing Systems*, volume 30. Curran Associates, Inc., 2017. URL https://proceedings.neurips.cc/paper_files/paper/2017/file/303ed4c69846ab36c2904d3ba8573050-Paper.pdf.
- Florian Sestak, Lisa Schneckenreiter, Johannes Brandstetter, Sepp Hochreiter, Andreas Mayr, and Günter Klambauer. Vn-egnn: E(3)-equivariant graph neural networks with virtual nodes enhance protein binding site identification, 2024. URL <https://arxiv.org/abs/2404.07194>.
- Noam M. Shazeer. Fast transformer decoding: One write-head is all you need. *ArXiv*, abs/1911.02150, 2019.
- Jake Topping, Francesco Di Giovanni, Benjamin Paul Chamberlain, Xiaowen Dong, and Michael M. Bronstein. Understanding over-squashing and bottlenecks on graphs via curvature, 2022. URL <https://arxiv.org/abs/2111.14522>.

- Petar Veličković, Guillem Cucurull, Arantxa Casanova, Adriana Romero, Pietro Liò, and Yoshua Bengio. Graph attention networks. In *International Conference on Learning Representations*, 2018. URL <https://openreview.net/forum?id=rJXMpikCZ>.
- Phil Wang. Equiformer - pytorch: Se3/e3 equivariant attention network. <https://github.com/lucidrains/equiformer-pytorch>, 2024. MIT License.
- Chen Hao Xia, Manasa Kaniselman, Alexandros Nikolaos Ziogas, Marko Mladenovic, Alexander Maeder, and Mathieu Luisier. Learning the hamiltonian of disordered materials with equivariant graph networks, 2025. URL <https://openreview.net/forum?id=t2f7sD9M7n>.
- Yuelin Zhang, Jiacheng Cen, Jiaqi Han, Zhiqiang Zhang, JUN ZHOU, and Wenbing Huang. Improving equivariant graph neural networks on large geometric graphs via virtual nodes learning. In *Forty-first International Conference on Machine Learning*, 2024. URL <https://openreview.net/forum?id=wWdkNkUY8k>.
- C. Lawrence Zitnick, Abhishek Das, Adeesh Kolluru, Janice Lan, Muhammed Shuaibi, Anuroop Sriram, Zachary W. Ulissi, and Brandon C. Wood. Spherical channels for modeling atomic interactions. *ArXiv*, abs/2206.14331, 2022.
- Álvaro Arroyo, Alessio Gravina, Benjamin Gutteridge, Federico Barbero, Claudio Gallicchio, Xiaowen Dong, Michael Bronstein, and Pierre Vandergheynst. On vanishing gradients, over-smoothing, and over-squashing in gnns: Bridging recurrent and graph learning, 2025. URL <https://arxiv.org/abs/2502.10818>.

A Dataset, Training, and Model Hyperparameters

Dataset All Chi-Geometry datasets used in our experiments contain 25,000 samples of simple type with species range = 15 and noise = True (see Section 3, Appendix B for details on dataset generation). The train/val/test split was set to 80/10/10.

Training Scheme and Model Training Scheme and Model: All models were trained using 500 epochs maximum, a 75-epoch early stopping criterion, 25-epoch learning rate decay with decay factor 0.5, and cross-entropy loss for classification. We used a learning rate of 0.0003, the Adam optimizer, gradient clipping with max L_2 -norm of 10, batch size of 32, and consistent dimensionalities for node features⁶. Additionally, we set the number of message-passing layers according to what we determine to be the minimum number that is sufficient to learn chirality.

Cross-Entropy Loss We use the weighted cross-entropy loss, which is a common loss function for machine learning classification tasks. It is defined as:

$$\text{CE} = - \sum_{t \in \{N/A, R, S\}} w_t p(t) \log(q(t))$$

where $p(t)$ is the true probability distribution, $q(t)$ is the model’s predicted probability distribution of a sample to belong to class N/A, R, or S, and w_t is the weight assigned to a certain class.

Class Weights to Counteract Dataset Imbalance The class weights for [N/A, R, S] in the cross-entropy loss are adjusted dynamically to counteract the effect of class imbalance in the datasets. For a dataset of simple type and chirality distance = D we know that $n_{N/A} = 3D \times (n_R + n_S)$, where n_i indicates the number of nodes of class i . The class weights mirror the imbalance by also being proportional to $(3 \times D)$. The general formula for class weights is:

$$[w_{N/A}, w_R, w_S] = [1.0, b + 3 \times D, b + 3 \times D]$$

where w_i represents the weight for class i and b is a constant that changes depending on the model architecture⁷.

⁶Node features are mapped to input dim of 40 before message-passing, hidden dim of 20 during message-passing, and output dim of 10 after message-passing.

⁷Preliminary tests indicated that the chosen values of b produced a sufficiently strong R/S classification signal, stable training, and avoided significant class imbalance. Specifically, we set $b = 10$ for the DimeNet++, Vanilla MPNN, Local E3NN, Global E3NN with feature engineering, and E3NN with virtual node models, $b = 6.0$ for the Global E3NN, and $b = 0.0$ for the SE(3)-Transformer.

B Chi-Geometry Data Generation

B.1 Sample Generation

Below, we elaborate on the creation process for samples generated by Chi-Geometry. The creation starts with the chiral center and proceeds layer by layer along the z axis, where the number of layers is the user supplied parameter chirality distance (a.k.a. D) (Section 3). Throughout this appendix section, we use $v \sim U(a, b)$ to indicate that a variable v is drawn uniformly at random from the interval $[a, b]$.

B.1.1 Simple Configurations

For the Chi-Geometry samples of simple type, each layer 1-D contains a triplet of nodes. The procedure goes as follows:

Setup:

We begin by randomly selecting node species for all nodes in the configuration. Specifically, we sample $4 + (D - 1)$ node species without replacement from the interval $[1, \text{species range}]$. This accounts for one species for the chiral center, three distinct species for the final layer, and $D - 1$ species for the $D - 1$ intermediate layers, where each intermediate layer shares the same species across all three of its nodes. Let S be this set of sampled node species and be zero-indexed (i.e. its indices go from zero to $D + 3$).

$$S \sim \text{UniformSubset}((1, \text{species range}), 4 + (D - 1))$$

Chiral Center:

Positions:

Noise Flag	p_c
noise = False	$(0, 0, 1)$
noise = True	$(r \cdot \cos \phi, r \cdot \sin \phi, 1)$

where p_c indicates the position of the chiral center, $r \sim U(0, 1)$, and $\phi \sim U(0, 2\pi)$.

Node Species:

$$x_c = S_0$$

For Layer in range (1, D):

Positions:

If Layer = 1, initialize $z = 1$.

1. Choose parameters

Noise Flag	Δz	r	θ
noise = False	0.5	1	$(0, \frac{2\pi}{3}, \frac{4\pi}{3})$
noise = True	$U(0.1, 1.5)$	$U(0.1, 1.0)$	$(0 + \epsilon_1, \frac{2\pi}{3} + \epsilon_2, \frac{4\pi}{3} + \epsilon_3)$

where $\epsilon_i \sim U(-\frac{\pi}{3.1}, \frac{\pi}{3.1})$ and $z \leftarrow z - \Delta z$.

2. Assign the 3 node positions

$$pos_{L,i} = (r \cdot \cos \theta_i, r \cdot \sin \theta_i, z), \quad i = 1, 2, 3$$

where L indicates the layer and i indicates the node index within a layer.

Node Species:

if layer < D:

$$x_{L,i} = S_L, \quad i = 1, 2, 3$$

else:

$$\text{sort_type} = \text{random}(\{\text{ascending}, \text{descending}\})$$

```

triplet = [SD+1, SD+2, SD+3]
order = argsort(triplet, sort_type)
xL,i = tripletorderi, i = 1, 2, 3

```

Edges:

```

if layer = 1:
    # Connect chiral center (0) to first layer atoms (1, 2, 3)
    edges.append([[0, i], [i, 0]]), i = 1, 2, 3
else:
    # Connect nodes from the current layer to the layer above
    idx_prev, idx_curr = 3 × (layer - 1) + 1, 3 × layer + 1
    edges.append([[idx_prev + i, idx_curr + i], [idx_curr + i, idx_prev + i]]), i = 1, 2, 3

```

The process will yield a total of 1 + 3D nodes (1 for the chiral center and 3 for each of the D layers).

B.1.2 Crossed Configurations

For the Chi-Geometry samples of crossed type, each layer 1-D contains a triplet of nodes. The procedure proceeds similarly to the simple samples, but randomizes the edge connections between layers:

Setup:

Identical to simple samples (Appendix B.1.1).

Chiral Center:

Identical to simple samples (Appendix B.1.1).

For Layer in range (1, D):

Positions:

Identical to simple samples (Appendix B.1.1).

Node Species:

Identical to simple samples (Appendix B.1.1).

Edges:

```

if layer = 1:
    # Connect chiral center (0) to first layer atoms (1, 2, 3)
    edges.append([[0, i], [i, 0]]), i = 1, 2, 3
else:
    # Connect nodes from the current layer to the layer above
    permutation = permute([0, 1, 2])
    idx_prev, idx_curr = 3 × (layer - 1) + 1, 3 × layer + 1
    edges.append([[idx_prev + permutation[i], idx_curr + permutation[i]],
                  [idx_curr + permutation[i], idx_prev + permutation[i]]]), i = 1, 2, 3

```

The process will yield a total of 1 + 3D nodes (1 for the chiral center and 3 for each of the D layers).

B.1.3 Classic Configurations

For the Chi-Geometry samples of classic type, each layer 1-D contains a quadruplet of nodes. The procedure goes as follows:

Setup:

We begin by randomly selecting node species for all nodes in the configuration. Specifically, we sample 5 + (D - 1) node species without replacement from the interval [1, species range]. This accounts for one species for the chiral center, four distinct species for the final layer, and D - 1 species for the D - 1 intermediate layers, where each intermediate layer shares the same species across all four of its nodes. Let S be this set of sampled node species and be zero-indexed (i.e. its indices go

from zero to $D + 4$).

$$S \sim \text{UniformSubset}((1, \text{species range}), 5 + (D - 1))$$

Chiral Center:

Identical to simple samples (Appendix B.1.1).

For Layer in range (1, D):

Positions:

If Layer = 1, initialize $z_{top} = z_{bot} = 1$.

1. Choose parameters

Noise Flag	Δz	r_{bot}, r_{top}	$\theta_{bot}, \theta_{top}$
noise = False	0.5	1,0	$(0, \frac{2\pi}{3}, \frac{4\pi}{3}), (0)$
noise = True	$U(0.1, 1.5)$	$U(0.1, 1.0), U(0.0, 1.0) (0 + \epsilon_1, \frac{2\pi}{3} + \epsilon_2, \frac{4\pi}{3} + \epsilon_3), (\epsilon_4)$	

where $\epsilon_i \sim U(-\frac{\pi}{3.1}, \frac{\pi}{3.1})$, $i = 1, 2, 3$, $\epsilon_i \sim U(-\pi, \pi)$, $z_{top} \leftarrow z_{top} + \Delta z$, and $z_{bot} \leftarrow z_{bot} - \Delta z$.

2. Assign the 4 node positions

$$pos_{L,i} = (r_{bot} \cos \theta_{bot,i}, r_{bot} \sin \theta_{bot,i}, z_{bot}), \quad i = 1, 2, 3,$$

$$pos_{L,4} = (r_{top} \cos \theta_{top}, r_{top} \sin \theta_{top}, z_{top}).$$

where L indicates the layer and i indicates the node index within a layer.

Node Species:

if layer < D:

$$x_{L,i} = S_L, \quad i = 1, 2, 3, 4$$

else:

```

sort_type = random({ascending, descending})
triplet = [SD+1, SD+2, SD+3, SD+4]
fourth = min(quadruplet)
triplet = quadruplet \ fourth (the quadruplet without the minimum node species)
order = argsort(triplet, sort_type)
xL,i = tripletorderi,  $i = 1, 2, 3$ 
xL,4 = fourth

```

Edges:

if layer = 1:

Connect chiral center (0) to first layer atoms (1, 2, 3, 4)

edges.append([[0, i], [i, 0]]), $i = 1, 2, 3, 4$

else:

Connect nodes from the current layer to the layer above

idx_prev, idx_curr = $4 \times (\text{layer} - 1) + 1, 4 \times \text{layer} + 1$

edges.append([[idx_prev+i, idx_curr+i], [idx_curr+i, idx_prev+i]]), $i = 1, 2, 3, 4$

The process will yield a total of $1 + 4D$ nodes (1 for the chiral center and 4 for each of the D layers).

B.1.4 Final Processing

After all D layers have been generated, we do the following final processing:

- Center: Translate the entire structure so that it is centered at the origin.
- Rotate: Apply a uniformly sampled rotation⁸ that has determinant 1 to the entire structure.

⁸We sample our rotation from the set of all 3-dimensional rotations with determinant +1 using SciPy.

These two operations are performed to remove any systematic orientation before the final positions, regardless of the choice of other parameters.

B.2 Node Labeling

The CIP rules Section 2.1 provide a procedure to label chiral centers with exactly four neighbors (as is the case for classic samples), but not for chiral centers with exactly three neighbors (as is the case for simple and crossed samples). To accommodate the simple and crossed sample types while adhering to consistent underlying principles, we mathematically formalize and generalize the CIP rules. We first define the scalar triple product and show its equivalence to the CIP rules, then apply the scalar triple product to label other sample types. For $a_1, a_2, a_3 \in \mathbb{R}^3$, the scalar triple product (STP) is defined as

$$a_1 \cdot (a_2 \times a_3).$$

The STP is a pseudoscalar, meaning its sign flips under reflections, but does not change under rigid rotations/translations. Since there is a one-to-one correspondence between reflection orientation and chirality, pseudoscalars are natural indicators of chirality.

B.2.1 Equivalence Between STP and CIP Rules

In this subsection, we show the equivalence between the clockwise/counterclockwise CIP labeling described in Section 2.1 and a certain STP. We derive the equivalence below:

Setup Let p_c be the position of the chiral center and p_1, p_2, p_3, p_4 denote the positions of its four substituents, ordered by CIP priority⁹ (p_1 is highest priority, p_4 is lowest). We prove that there is a 1-to-1 correspondence between the CIP assignment and the sign of $(p_4 - p_c) \cdot [(p_2 - p_1) \times (p_3 - p_2)]$.

Orient Without loss of generality, we translate and rotate the structure so that $p_c = 0$ and p_4 lies along the positive z -axis, meaning $p_4 = (0, 0, z^+)$ where $z^+ \in \mathbb{R}^+$. By CIP convention, the structure is viewed such that the lowest priority substituent is directly behind the chiral center, at a far enough viewpoint to see the entire structure. Since the lowest priority substituent and chiral center are located at $(0, 0, z^+)$ and $(0, 0, 0)$, respectively, the viewpoint must be located $(0, 0, z^-)$, where $z^- \in \mathbb{R}^-$ and is sufficiently negative to view the other three neighbors.

Substitute Plugging p_4 and p_c into our STP formula, we have:

$$(0, 0, z^+) \cdot [(p_2 - p_1) \times (p_3 - p_2)].$$

It is clear that the sign of the STP depends solely on the sign of the z -component of the cross product.

Equivalence Viewed from the $(0, 0, z^-)$ perspective defined earlier, the clockwise / counterclockwise orientation traced by $p_4 \rightarrow p_3 \rightarrow p_2$ also has a one-to-one correspondence with the sign of the z -component of the cross product $[(p_2 - p_1) \times (p_3 - p_2)]$. A positive z -component indicates a clockwise orientation, while a negative z -component indicates counterclockwise. Therefore, we have a 1-to-1 relation between the sign of the previously defined STP and labeling by CIP rules, namely: Positive STP \iff Clockwise, Negative STP \iff Counterclockwise.

B.2.2 Labeling by STP

Having established that the sign of the STP provides a formal labeling rule, we now apply it to the other sample types in Chi-Geometry. First, we must index the nodal positions to be used in the STP. To do so, note that each sample consists of the chiral center and D layers of nodes (see Appendix B.1). Then, index the positions so that p_c is the position of the chiral center, and $p_{L,i}$ is the position of the i -th priority node ($i = 1$ is highest priority) of layer L . We then define the respective STP for each sample type:

⁹CIP priority is determined by first ranking from highest to lowest atomic number. If any share the same atomic number, the process continues by comparing additional atomic attributes and, if necessary, recursively comparing attributes of the substituents' neighbors until a difference is found (see Section 2.1).

$$\text{Classic: STP} = (p_{1,4} - p_c) \cdot [(p_{1,2} - p_{1,1}) \times (p_{1,3} - p_{1,2})],$$

$$\text{Simple: STP} = (p_c - p_{1,1}) \cdot [(p_c - p_{1,2}) \times (p_c - p_{1,3})],$$

$$\text{Crossed: STP} = (p_c - p_{D,1}) \cdot [(p_c - p_{D,2}) \times (p_c - p_{D,3})].$$

where D is the chirality distance specified in sample creation (see Section 3, Appendix B.1).

B.3 What the Different Chi-Geometry Sample Types are Testing

In Chi-Geometry, the Classic/Simple samples and the Crossed samples test for different capabilities of the GNN, which is now clear given the detailed explanation of the sample creation (Appendix B.1) and node labeling (Appendix B.2). First, note that in all samples, the chirality is determined by the relative (1) geometry and (2) priority of the nodes whose positions are input to the STP (call these the STP nodes). In classic and simple samples, the STP nodes are directly connected to the chiral center, so the relevant geometry is strictly local. However, because all nodes in the intermediate layers share the same node species (by construction), the priority of the STP nodes depends on the node species of the nodes in the final layer. Hence, the priority is determined by a variable-range interaction whose hop distance equals the number of layers (see Section 2.1 for more detail on how the priority is determined). On the other hand, the crossed samples draw all three STP nodes from the final layer, which clearly makes both the relative geometry and priority variable-range from the chiral center. Since the number of layers is selected by the user in Chi-Geometry, the hop distance of the variable-range interactions is tunable. In summary, the classic and simple samples test a GNN’s ability to capture short-range geometry and variable-range node attributes, while the crossed samples test a GNN’s ability to capture variable-range geometry and node attributes.

B.4 Guaranteeing Chiral Centers in the Samples

Each graph constructed by Chi Geometry is engineered to contain exactly one chiral center, labeled R or S. In this section, we show that (i) the initial construction of a sample yields exactly one chiral center and (ii) all subsequent transformations of that sample preserve the labeling of the chiral center.

B.4.1 Setup

To be a chiral center, a node must have a certain number of neighbors (3 for simple/crossed samples and 4 for classic), the CIP ordering of those neighbors must be well-defined, and the requisite STP used to assign the label of R or S must be nonzero.

First, note that by construction, each Chi-Geometry sample will contain exactly one node with the correct number of neighbors to be a chiral center. Second, see that in Chi-Geometry samples, the chiral center connects to a first layer, then each first-layer node connects 1-to-1 to a second layer node, and so on until the final layer. Because every intermediate layer is homogeneous in their node species, the decisive tie-break in CIP ordering depends on the node species of the final layer (see Section 2.1 for more detail on CIP ordering). Since this final layer contains all distinct node species, the ordering is well-defined. Finally, we must show that the respective STP of each sample type is nonzero. To show this, we first prove a general case given some assumptions and then show that each of the sample types created by Chi-Geometry satisfies those assumptions.

In the general case, assume we have vectors $v_1, v_2, v_3 \in \mathbb{R}^3$, where:

- v_1 contains a nonzero z -component
- v_2, v_3 lie in the xy -plane
- v_2, v_3 are not collinear

We will demonstrate that $\text{STP}(v_1, v_2, v_3)$ is nonzero. First, note that $(v_2 \times v_3) = (0, 0, z_{\text{cross}})$ where $z_{\text{cross}} \neq 0$ because v_2, v_3 lie in the xy -plane. Then, it clearly follows that $v_1 \cdot (0, 0, z_{\text{cross}}) \neq 0$ because v_1 has a nonzero z -component. Thus, $\text{STP}(v_1, v_2, v_3) = v_1 \cdot (v_2 \times v_3) \neq 0$. Now, we show that each sample type fulfills the assumptions above. In order for us to do so, first note these two facts:

1. $\text{STP}(v_1, v_2, v_3) = \det(v_1, v_2, v_3)$
2. $\det(v_1, v_2, v_3) = \det(v_1, v_2 + v_1, v_3 + v_1)$

Then, observe the following STPs for each sample type:

1. **Classic:** $\text{STP}(p_{1,4} - p_c, p_{1,2} - p_{1,1}, p_{1,3} - p_{1,2})$.
2. **Simple:** $\text{STP}(p_c - p_{1,1}, p_c - p_{1,2}, p_c - p_{1,3}) = \det(p_c - p_{1,1}, p_c - p_{1,2}, p_c - p_{1,3}) = \det(p_c - p_{1,1}, p_{1,1} - p_{1,2}, p_{1,1} - p_{1,3}) = \text{STP}(p_c - p_{1,1}, p_{1,1} - p_{1,2}, p_{1,1} - p_{1,3})$.
3. **Crossed:** $\text{STP}(p_c - p_{D,1}, p_c - p_{D,2}, p_c - p_{D,3}) = \det(p_c - p_{D,1}, p_c - p_{D,2}, p_c - p_{D,3}) = \det(p_c - p_{D,1}, p_{D,1} - p_{D,2}, p_{D,1} - p_{D,3}) = \text{STP}(p_c - p_{D,1}, p_{D,1} - p_{D,2}, p_{D,1} - p_{D,3})$.

For any of the sample types above, we know that v_1 has a z -component and v_2, v_3 lie in the xy -plane by construction (see Appendix B.1). Define the positions that are used in v_2, v_3 as P_1, P_2, P_3 (there are always 3 distinct positions in any of the sample types). Note that for every sample in Chi-Geometry we can label the points such that $v_2 = P_1 - P_2, v_3 = P_1 - P_3$ up to signs, so proving these two difference vectors are non-collinear therefore establishes the result for every sample type. We know by construction that P_1, P_2, P_3 all lie on a circle of radius $r > 0$ (see Appendix B.1). For P_1, P_2, P_3 to be collinear while lying on the same circle with radius $r > 0$, at least two of the points must be equivalent, which implies their angles must be equivalent. But, their angles cannot be equivalent because $\theta = (0 + \epsilon_1, \frac{2\pi}{3} + \epsilon_2, \frac{4\pi}{3} + \epsilon_3)$ where $\epsilon_i \in (-\frac{\pi}{3.1}, \frac{\pi}{3.1})$ for $i = 1, 2, 3$. Therefore, P_1, P_2, P_3 are not collinear. Then, assume for the sake of contradiction that P_1, P_2, P_3 are not collinear, but $P_1 - P_2$ and $P_1 - P_3$ are. Since $P_1 - P_2$ and $P_1 - P_3$ are collinear, it follows that for $c \in \mathbb{R}$, $c(P_1 - P_2) = P_1 - P_3 \rightarrow P_3 = [(1 - c)P_1] + cP_2$. But, this contradicts the fact that P_1, P_2, P_3 are not collinear. Therefore, by contradiction, $P_1 - P_2$ and $P_1 - P_3$ must not be collinear.

B.4.2 Transformations

In this subsection, we show that $\det(v_1, v_2, v_3)$ (which is equal to $\text{STP}(v_1, v_2, v_3)$) remains unchanged by the transformations after the initial sample construction. Since the STP is used to assign chirality labels, this implies that the transformations do not corrupt the label assignment. First, note that:

- For every sample type in Chi-Geometry, all v_i ($i = 1, 2, 3$) in that sample type’s respective STP are relative vectors.
- For any two square matrices $A, B \in \mathbb{R}^{n \times n}$, $\det(AB) = \det(A) \det(B)$

Then, for the two transformations (centering + rotation):

1. **Centering:** translate the structure by $t \in \mathbb{R}^3$ so that the structure is centered at the origin.
 - The determinant is unchanged by translation of the structure because relative vectors are unchanged by translations.
2. **Rotation:** apply a random rotation $A \in \mathbb{R}^{3 \times 3}$ where $\det(A) = 1$.
 - Rotating the positions will correspondingly rotate the relative vectors. Denote $\det(v_1, v_2, v_3)$ as $\det(V)$ and $\det(Av_1, Av_2, Av_3)$ as $\det(AV)$. Then, the determinant of the rotated structure $\det(AV) = \det(A) \cdot \det(V) = \det(V)$. Therefore, the determinant is unchanged by rotation.

Therefore, the STP (and equivalently the chirality labeling) is unchanged by the centering and random rotation applied after initial sample construction.

C Equivariance

Definition Equivariance is a mathematical concept in group and representation theory, with strong applications for ML models in molecular, materials, and biological prediction tasks. We use the following definition of equivariance by Kondor and Trivedi [2018]:

Let G be a group and X_1, X_2 be two sets with corresponding G -actions

$$T_g : X_1 \rightarrow X_1, \quad T'_g : X_2 \rightarrow X_2.$$

Let V_1 and V_2 be vector spaces, and \mathbb{T}, \mathbb{T}' be the induced actions of G on $L_{V_1}(X_1)$ and $L_{V_2}(X_2)$.

We say that a map $\phi : L_{V_1}(X_1) \rightarrow L_{V_2}(X_2)$ is equivariant with the action of G (or G -equivariant for short) if $\phi(\mathbb{T}_g f) = \mathbb{T}'_g \phi(f) \quad \forall f \in L_{V_1}(X_1)$ for any group element $g \in G$.

Succinctly, equivariant means that transformations and mappings commute. Invariance is the special case where $\mathbb{T}'_g = \text{id}_{L_{V_2}(X_2)}$ (the identity). In other words, applying the G -action does not change the output of ϕ .

Additionally, we define an equivalence class under the G -action as the set of all elements that can be mapped to one another by transformations in G . Any single element from this set may serve as its representative.

Examples Some real-world examples of equivariance in chemistry and materials science include:

1. **Free Energy:** Free energy remains invariant under any rotation, translation, or reflection.
2. **Interatomic Forces:** Interatomic forces rotate correspondingly with the structure, making them equivariant to rotations.
3. **Chiral Center R/S Label:** A chiral center’s tag (R or S) is invariant to translations and rotations, and equivariant to reflections.

Impact When configured correctly, equivariant models inherently respect the symmetries of their prediction task/s. By treating all elements in an equivalence class as transformed versions of a single representative, these models reduce the dimensionality of the functional space in which they learn. This translates into an easier learning task, resulting in improved performance and learning efficiency [Jumper et al., 2021, Merchant et al., 2023, Batzner et al., 2022, Batatia et al., 2022, Morehead and Cheng, 2022].

D Over-squashing Analysis

The following method is used to perform an analysis of over-squashing in the experiment from Section 4.1. In this experiment, we trained the model on nine distinct datasets parametrized by chirality distance $D \in \{1, 2, \dots, 9\}$. The chirality distance parameter controls how many connection ‘hops’ separate the chiral center from the substituent nodes which determine its chiral tag. Once each model is trained, we analyze over-squashing on its corresponding dataset by measuring the gradients of node features with respect to the chiral center classification loss.

The over-squashing analysis proceeds in three main steps:

1. BFS for Hop Distances

Let c be the chiral center in the graph $G = (V, E)$. For each node $v \in V$, define its hop distance $f(v)$ to c as the length of the shortest path from c to v . For example, $f(c) = 0$, $f(v) = 1$ if v is directly connected to c , and so on.

2. Gradient Calculation Let CE be the cross-entropy classification loss computed only on the chiral center c . Each node v has a feature vector x_v . We backpropagated on CE to find $\nabla_{x_v} \text{CE}$, then measure node v ’s importance via its respective gradient’s L_2 -norm:

$$g(v) = \|\nabla_{x_v} \text{CE}\|_2.$$

We collected this value across all nodes for all graphs in the dataset.

3. Aggregation and Normalization For each distance $d \in \{1, 2, \dots, D\}$, we averaged $g(v)$ over all nodes v with $f(v) = d$. Then, we normalized these averages so they sum to 1:

$$g(d) = \frac{1}{|\{v : f(v) = d\}|} \sum_{f(v)=d} g(v), \quad \hat{g}(d) = \frac{g(d)}{\sum_{d=1}^D g(d)}.$$

The value of $\hat{g}(d)$ indicates the relative importance of nodes at hop distance d from the chiral center. For any Chi-Geometry dataset generated with chirality distance D , the nodes exactly D hops away from the chiral center determine the center’s R/S label. Therefore, a well-trained model should assign these deciding nodes a large share of the gradient. If the relative gradient of the deciding nodes (represented by $\hat{g}(D)$) plummets as D grows, it indicates that over-squashing is taking place.

E Computational Cost and Hardware

Wall-clock durations were computed as the difference between the configuration save timestamp (immediately before training) and the final-results timestamp (immediately after training/evaluation). All runs were executed on a MacBook Pro (14 inch) with an Apple M3 Pro CPU and 36 GB of RAM. The total runtime across all experiments is **313.16 hours**.

Table 6: Training durations (decimal hours) for $D = 1 \dots 9$.

Model	D=1	D=2	D=3	D=4	D=5	D=6	D=7	D=8	D=9	Total
E3NN Virtual Node	1.40	1.42	4.78	4.62	1.75	4.80	2.28	2.55	3.32	26.92
Global E3NN (Feat. Eng.)	2.18	3.65	4.92	5.60	19.00	20.65	27.08	50.98	59.00	193.23
Local E3NN	3.23	5.13	5.43	8.30	9.60	3.90	4.15	3.58	4.10	47.42

Table 7: Training durations (decimal hours) for repetitions $R = 1 \dots 10$ at $D = 1$.

Model	R=1	R=2	R=3	R=4	R=5	R=6	R=7	R=8	R=9	R=10	Total
Global E3NN	1.02	0.98	1.12	1.22	1.90	2.20	2.27	1.57	2.33	2.23	16.84
SE(3)-Transformer	2.97	3.07	2.98	2.65	2.57	2.55	2.57	2.55	2.57	2.55	27.03
Vanilla MPNN	0.13	0.13	0.12	0.13	0.13	0.40	0.15	0.15	0.23	0.15	1.72